JOURNAL OF MATERIALS SCIENCE 27 (1992) 3068–3074

Influence of SiC reinforcement on precipitation and hardening of a metal matrix composite

J.-P. COTTU, J.-J. COUDERC, B. VIGUIER, L. BERNARD
Laboratoire de Physique des Solides associé au CNRS (L.A. 74), UPS et INSA, Avenue de Rangueil, 31077 Toulouse cedex, France

The influence of fibre reinforcement (10 vol% SiC fibres) on the precipitation and hardening behaviour of a metal matrix composite was studied using microhardness tests and transmission electron microscopy observations. It was shown that the hardening kinetics is enhanced by the SiC reinforcement due to the fact that precipitation preferentially develops on dislocation lines. Moreover, the high-temperature deformation strongly increases the precipitation rate as the material is reinforced.

1. Introduction

The material studied is a metal matrix composite (MMC) made of an AS7G06 aluminium alloy reinforced with chopped SiC fibres (about 10–15 μm diameter and 3–6 mm long). As with most light alloys, the alloy composing the matrix is able to undergo thermal treatment for precipitation hardening.

During high-temperature tensile deformation tests intended to simulate the forging conditions, Coutand *et al.* [1] reported a noticeable difference in the plastic behaviour of the reinforced and unreinforced material for identical thermal treatments.

The aim of this paper is a better understanding of the origin of this difference; in particular, the influence of the fibre reinforcement on the precipitation and hardening behaviour of the material deserves special attention.

Precipitation hardening in Al–Si–Mg ternary alloys has already been investigated by several authors [2–4]. Most agree that the precipitated phase is Mg_2Si, but very often its structure is not precisely defined. According to Brichet [2], a four-stage process is operating in the 0.8 at% Mg_2Si–Al pseudo-binary alloy:

(i) precipitation of Guinier–Preston zones (needles about 10 nm long);

(ii) intermediate phase β′-Mg_2Si, together with a homogeneous precipitation;

(iii) intermediate phase β′-Mg_2Si together with a heterogeneous precipitation;

(iv) equilibrium phase β-Mg_2Si, cfc structure (a = 0.639 nm) rod- or plate-shaped (0.1 μm × 1 μm).

The orientation relationships between β-Mg_2Si and the aluminium matrix have been determined:

$$(0\,0\,1)_{\beta}//(0\,0\,1)_{Al}$$

$$[1\,1\,0]_{\beta}//[1\,0\,0]_{Al}$$

and the β′ intermediate phase (hexagonal structure, a = 0.705 nm, c = 0.405 nm) has been found by Jacobs [3] in a 1.2 at% Mg_2Si–Al alloy with the following orientation relationships:

$$(0\,0\,1)_{\beta'}//(1\,0\,0)_{Al}$$

$$[1\,0\,0]_{\beta'}//[0\,1\,\bar{1}]_{Al} \text{ or } [0\,1\,1]_{Al}$$

When the β′-Mg_2Si rods lose their coherency with respect to the matrix, a structural modification is observed, leading to another hexagonal unit cell, a = 0.705 nm and c = 1.251 nm.

Finally, Dumolt *et al.* [4] have shown that the β′ phase structure strongly depends on the matrix composition: in a 6061 Al alloy, the β′ phase can be described by an orthorhombic cell (a = 1.8 nm, b = 1.04 nm, c = 0.405 nm) or a hexagonal one (a = 1.04 nm, c = 0.405 nm).

It is worth noting that in all cases, the precipitates are rod- or needle- shaped and have their axial direction parallel to $\langle 1\,0\,0\rangle_{matrix}$.

2. Experimental procedure

The MMC was produced in the Laboratoire de Chimie du Solide (Université de Bordeaux, France) by rheocasting. This process made it possible to destroy the dendritic structure of the Al–Si eutectic that is unfavourable to reliable mechanical properties.

Table I gives the values of the Young's and shear moduli, and the Brinell hardness [5] for T6 MMC (i.e. 4 h annealed at 540 °C, water quenched and aged 8 h at 150 °C).

In the present study, Vickers microhardness tests were performed using a Durimet Leitz with a 10 g direct loading. The loading time was 15 s. Each microhardness value was obtained after statistical treatment of the experimental data.

The samples for transmission electron microscopy (TEM) studies were mechanically ground, then thinned by ion-milling. The observations were made in a Jeol-200CX electron microscope operated at 200 kV. In order to obtain a semi-quantitative analysis of

0022–2461 © *1992 Chapman & Hall*

TABLE I Mechanical data for T6 materials (4 h at 540 °C, water quenched and 4 h at 180 °C) at room temperature [5]

	Fibre volume (%)		
	0	8	15
Young's modulus (GPa)	73	79	85
Shear modulus (GPa)	27	29.5	32
Brinell hardness (diameter 10 mm; 10 kN)	122	123	126

precipitates, thin film X-ray spectroscopy was performed using the same electron microscope fitted with an energy dispersive lithium-drifted silicon detector, a standard STEM attachment and an EDAX 9100 spectrum analyser unit (TEM-SCAN Service of the Université Paul Sabatier, Toulouse).

3. Results

3.1. Microhardness tests

These tests were performed on two sets of samples: the AS7G06 matrix and a 10 vol % SiC-reinforced material. The specimens were first annealed for 8 h at 540 °C (setting into solution), then water quenched and finally aged at 180 °C for a time ranging from 1–144 h. The Vickers hardness was measured for various ageing times (Fig. 1a and b). From these results, it is noted that the matrix reinforcement strongly enhances the hardening rate; thus the MMC is more rapidly hardened than the unreinforced matrix. Moreover the height of the microhardness curves shows that the hardening is more important. Christman and Suresh [6] have drawn similar conclusions for a SiC reinforced 2024 Al alloy.

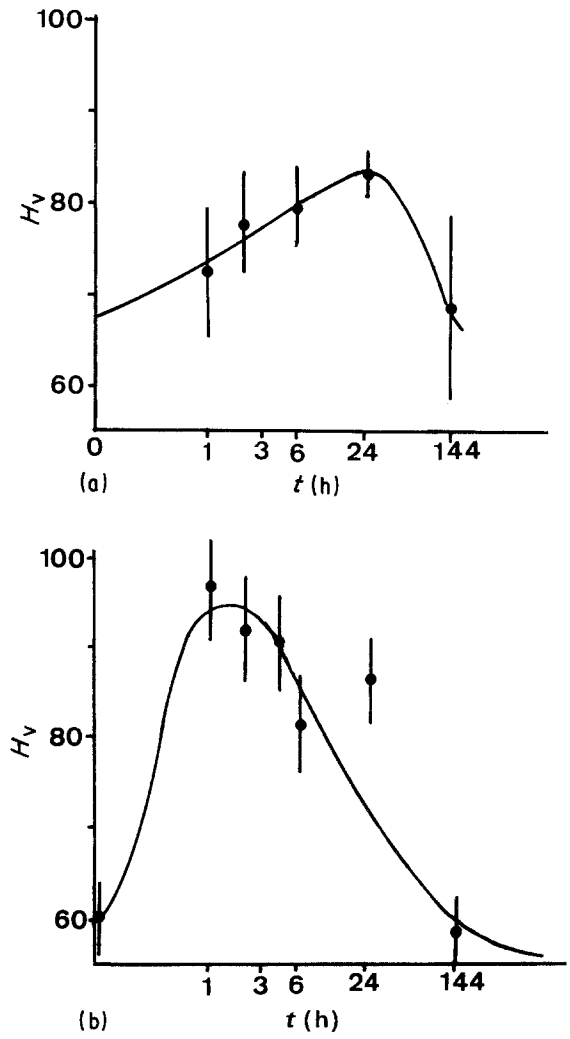

Figure 1 Vickers microhardness, H_v, versus ageing time, t, for (a) AS7G06 aluminium alloy, (b) 10% SiC-reinforced composite.

3.2. TEM observations

3.2.1. Precipitate structure and morphology

We are mainly interested in two types of precipitate that generally are found to coexist in our samples.

(i) Rounded precipitates of small size (about 2–10 nm diameter). No extra spots corresponding to these precipitates have been observed on the electron diffraction patterns. In addition, the small size of these precipitates, which are probably Mg_2Si, does not allow X-ray microanalysis to be performed.

(ii) Needle-shaped precipitates. These range in length from 50 nm to a few micrometres according to the thermal treatment. They are oriented with their axis parallel to $\langle 1\,0\,0\rangle_{matrix}$.

The structure of these precipitates was investigated on a 10% SiC-reinforced composite, strained to failure at 565 °C ($\sigma_F = 4.5$ MPa, $\varepsilon_F = 6\%$). Selected-area electron diffraction patterns show that these precipitates have a hexagonal structure (Fig. 2) with $a = 0.42 \pm 0.01$ nm and $c = 0.68 \pm 0.015$ nm. This structure is not consistent with the data found in the literature for Mg_2Si (cf. Section 1).

X-ray microanalysis was performed on these precipitates: they are significantly richer in silicon and magnesium than the matrix. Unfortunately, the minimum size of the electron microprobe ($\simeq$ 10–20 nm) did not allow avoidance of simultaneous analysis of the surrounding matrix, and particularly the AlK_α radiation was always very important. Thus a quantitative analysis of the precipitates was not possible. Nevertheless, it was noted that the atomic ratio Mg/Si was about unity and did not, therefore, correspond to the Mg_2Si chemical formula.

Some large precipitates (rods or plates) seem to have lost their coherency with respect to the matrix. They have not been studied precisely.

Finally, rounded silicon precipitates (diameter 5–50 nm) were also observed in some matrix grains. They have no definite orientation relationships with the matrix and are easily identified by the existence of Debye–Scherrer rings in the electron diffraction patterns.

3.2.2. Ageing dependence of the precipitation and dislocation structure

TEM observations were carried out on the two sets of samples (AS7G06 matrix and reinforced material) used for microhardness tests with various ageing times (1–144 h at 180 °C).

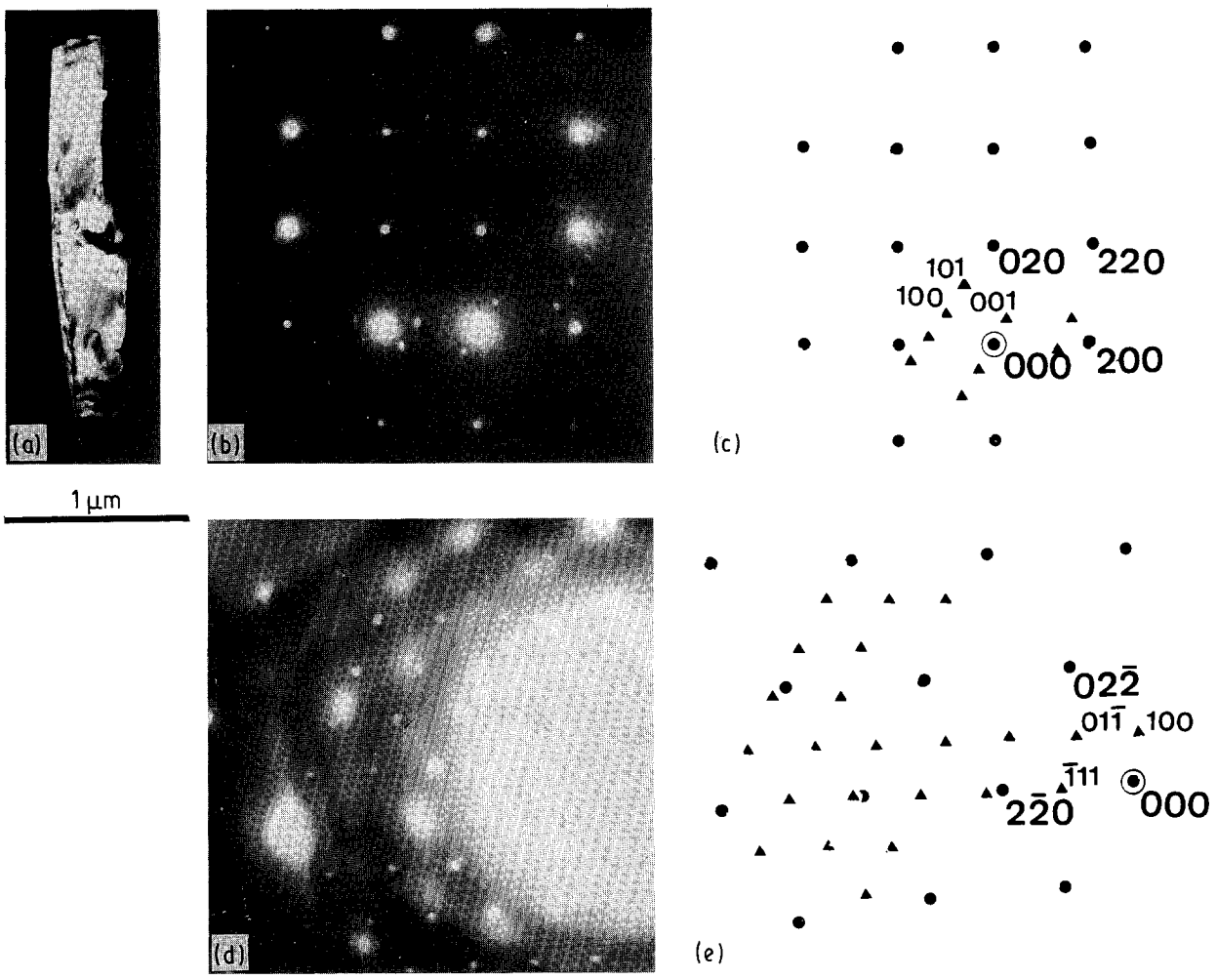

Figure 2 (a) Dark-field electron micrograph showing a rod-shaped precipitate in a composite strained until failure at 565 °C. The operative reflection belongs to the precipitate. The precipitate axis is parallel to $[0\,1\,0]_{matrix}$. (b) Electron diffraction pattern corresponding to (a). (c) Interpretation of electron diffraction pattern in (b). (●) Matrix, cfc structure, electron beam parallel to [0 0 1]; (▲) precipitate, hexagonal structure, electron beam parallel to [0 1 0]. (d) Electron diffraction pattern of matrix and precipitate. (e) Interpretation of electron diffraction pattern in (d). (●) Matrix, electron beam parallel to [1 1 1]; (▲) precipitate, electron beam parallel to [0 1 1].

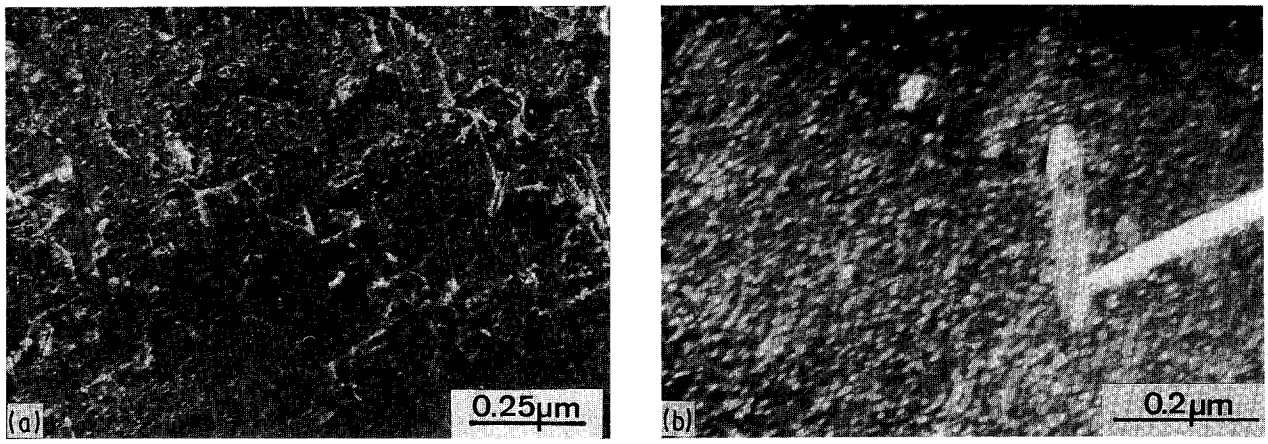

Figure 3 Electron micrographs of ⟨1 1 1⟩ weak beam dark-field AS7G06 aluminium alloy, (a) after 9 h ageing, (b) after 144 h ageing.

3.2.2.1. Unreinforced AS7G06 matrix. After a 9 h ageing, that is near to the maximum of microhardness, we observe a relatively small density of dislocations ($\simeq 5 \times 10^8$ cm^{-2}), a very homogeneous distribution of rounded precipitates of small size (about 2 nm diameter) or needle-shaped (3 nm × 10 nm) and some rod-shaped precipitates (2 nm × 200 nm) (Fig. 3a). After 144 h ageing, which corresponds to a decrease of the microhardness, the dislocation density is approximately the same, but the small rounded precipitates

have coarsened and their density has decreased (Fig. 3b). The rod-shaped ones also have increased in size (40 nm × 500 nm).

3.2.2.2. 10% SiC-reinforced composite. After a 9 h ageing (Fig. 4a), the precipitate distribution is quite homogeneous and the dislocation density is about 10^9 cm^{-2}, higher than that observed in the unreinforced matrix for the same thermal treatment, but the size of both rod-shaped precipitates (10 nm × 300 nm) and rounded ones (about 4 nm diameter) is increased.

After 144 h ageing (Fig. 4b), corresponding to a weaker microhardness of the material, the precipitate arrangement is very heterogeneous: the size of the rods reaches 40 nm × 1000 nm and the small precipitates are about 6 nm diameter.

Thus TEM observations confirm that the precipitate coarsening and heterogeneous distribution is closely correlated with the hardness values of the material after a few hours ageing.

On the other hand, comparing Figs 3a and 4a, 3b and 4b which correspond to the same ageing time, it is clear that precipitation is more rapid in the reinforced material: both types of precipitate are larger in Fig. 4a and b.

3.2.3. Strain effect on precipitation: TEM observations

Strain effect on precipitation has been investigated on the same series of samples (matrix and composite). For each set of specimens, the precipitation structure and dislocation landscape were studied:

1. in an as-solidified sample;
2. in a T6 sample, i.e. solution treated by annealing for 4 h at 540 °C, then water quenched and aged 8 h at 150 °C;
3. in a sample strained to failure at high temperature. This thermal process is intended to simulate the forging conditions.

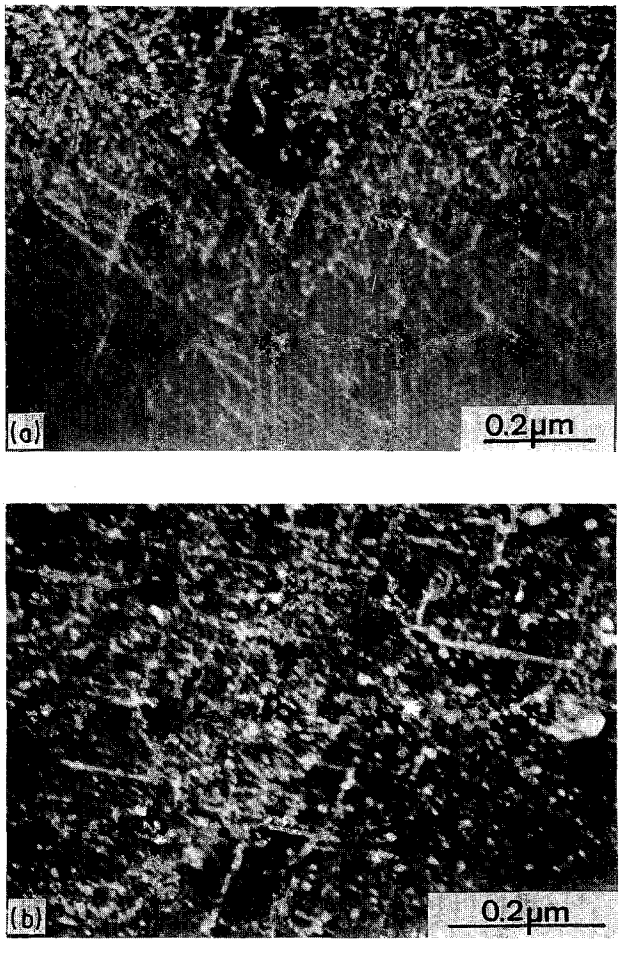

Figure 4 Electron micrographs of ⟨1 1 1⟩ weak beam dark-field SiC-reinforced composite, (a) after 9 h ageing, (b) after 144 h ageing.

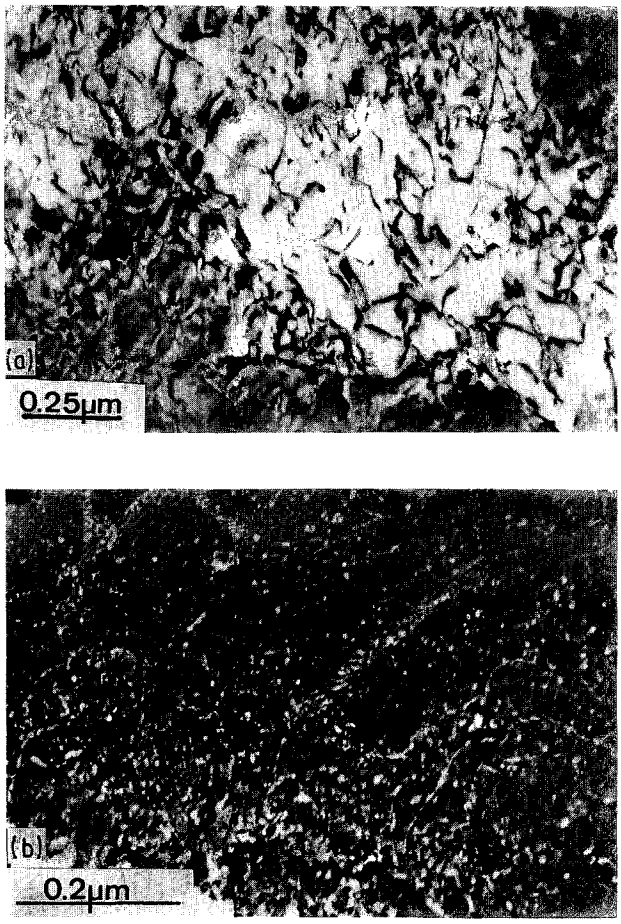

Figure 5 Electron micrographs of as-solidified AS7G06 matrix. (a) Bright field, high dislocation density (≅ 10^{10} cm^{-2}); (b) ⟨1 1 1⟩ weak beam dark-field, small precipitates (1–5 nm) and rod-shaped ones.

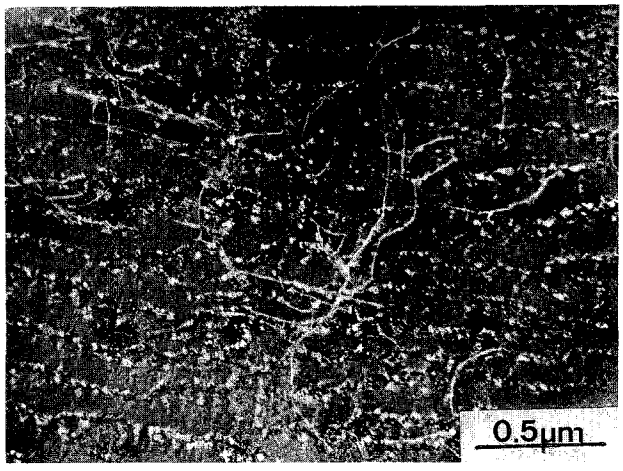

Figure 6 Electron micrographs of ⟨1 1 1⟩ weak beam dark-field as-solidified composite. Dislocations and small precipitates (about 5 nm).

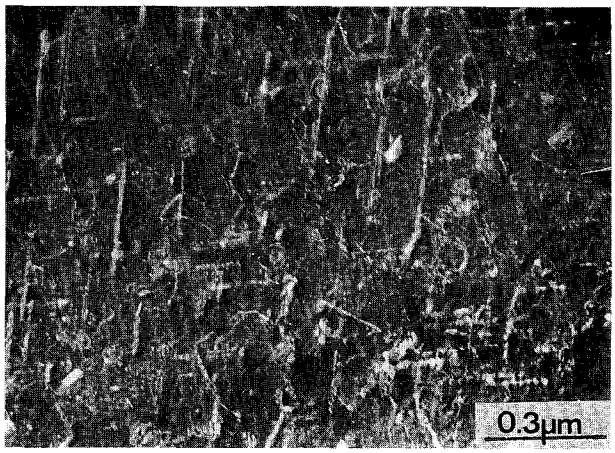

Figure 7 Electron micrographs of ⟨1 1 1⟩ weak beam dark-field T6 matrix. Two families of rod-shaped precipitates.

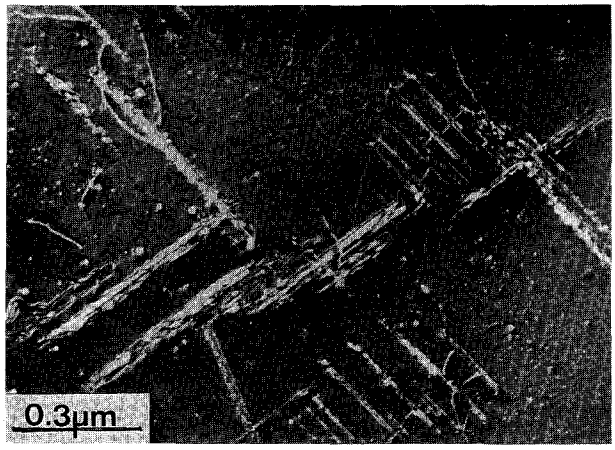

Figure 8 Electron micrographs of ⟨1 1 1⟩ weak beam dark-field T6 composite. The rod-shaped precipitates are bigger than in Fig. 7.

3.2.3.1. As-solidified samples. In the AS7G06 matrix (Fig. 5a and b), a high density of dislocations is observed (10^{10} cm^{-2}). Small rounded precipitates (about 1–5 nm diameter) rather homogeneously distributed are also visible. The rod-shaped precipitates are comparatively rare.

In the reinforced composite (Fig. 6), the dislocation density is very similar ($\simeq 10^{10}$ cm^{-2}). Nevertheless the precipitates are more heterogeneously distributed and their mean size is increased: the small rounded ones are about 5 nm diameter and the rod-shaped ones have a mean size of about 50 nm × 1000 nm.

3.2.3.2. T6 samples. In the matrix (Fig. 7), the dislocation density has decreased ($\simeq 10^{9}$ cm^{-2}) and rod-shaped precipitates (mean size 50 nm × 500 nm) are much more numerous. The small rounded precipitates have approximately the same size (about 4 nm diameter) as before.

In the composite (Fig. 8) the dislocation density is virtually the same as in the matrix ($\simeq 10^{9}$ cm^{-2}) but the rods are longer (50 nm × 1000 nm) and decorate the dislocations. The arrangement of rounded precipitates seems to be heterogeneous and no significant variation is observed in their mean size, as compared to the matrix.

3.2.3.3. Strained samples. We first studied an AS7G06 aluminium alloy strained to fracture at 520 °C ($\varepsilon_R = 160\%$, $\sigma_R = 9.8$ MPa): a network of nearly straight dislocations (density $\simeq 2 \times 10^{9}$ cm^{-2}) parallel to ⟨1 1 0⟩ is observed (Fig. 9a). Rod-shaped precipitates (Fig. 9b) have a mean size of about 20 nm × 300 nm and the rounded ones are about 8 nm diameter. The precipitation structure is thus coarser than in the same sample either as-solidified or T6.

In an AS7G06 matrix strained at higher temperature (545 °C) ($\varepsilon_R = 123\%$, $\sigma_R = 7$ MPa), no preferential directions are observed for dislocation lines and their density remains approximately the same (Fig.

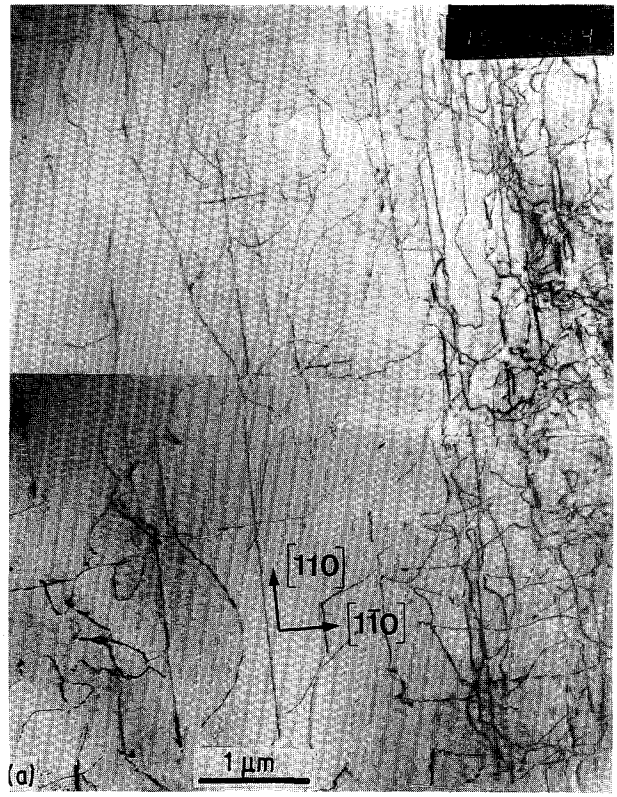

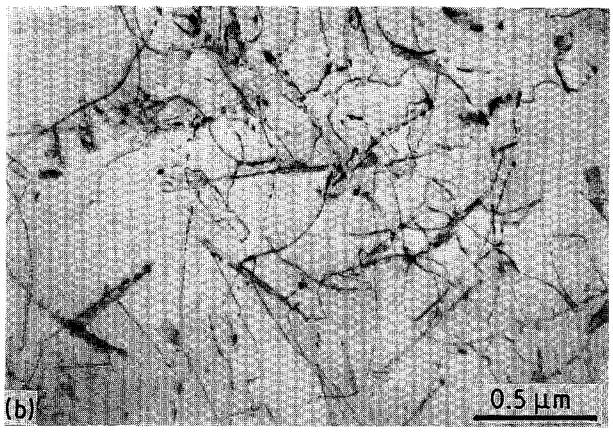

Figure 9 Bright-field electron micrographs of a matrix strained to failure at 520 °C. (a) Dislocation lines are parallel to ⟨1 1 0⟩; (b) rod-shaped precipitates.

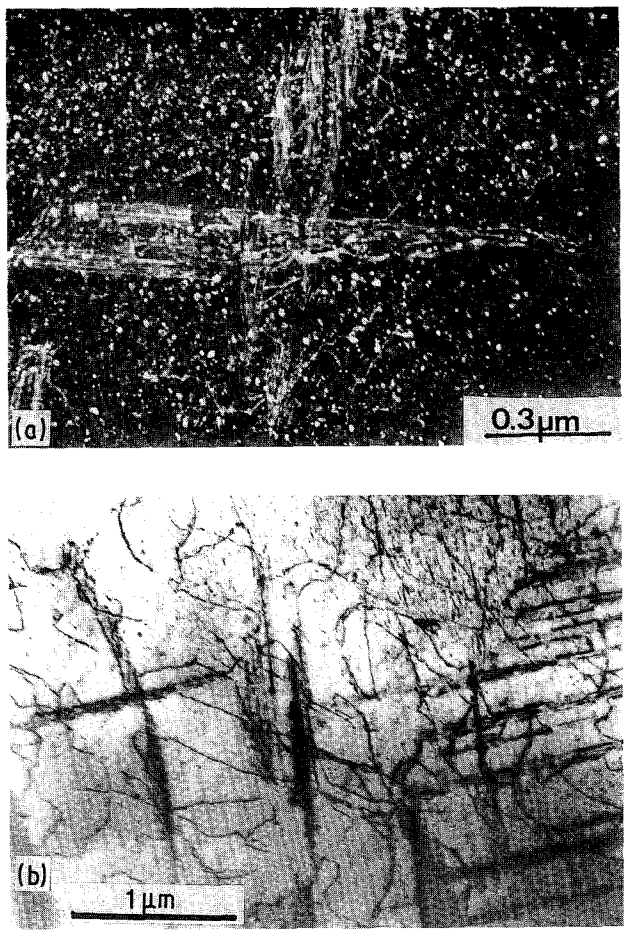

Figure 10 Electron micrographs of matrix strained to failure at 545 °C. (a) ⟨1 1 1⟩ weak beam dark-field; (b) Bright field.

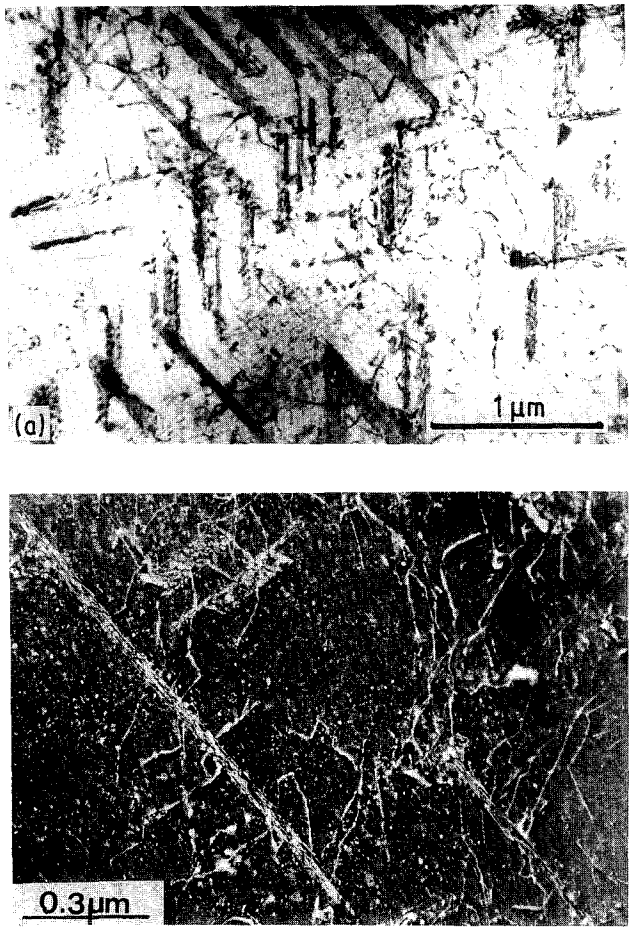

Figure 11 Electron micrographs of a composite strained to failure at 565 °C. (a) Bright field; (b) ⟨1 1 1⟩ weak beam dark-field.

10). The rod-shaped precipitates are bigger (mean size 100 nm × 1000 nm) and the rounded ones (5–10 nm diameter) are homogeneously distributed.

In the composite strained to failure at 565 °C ($\varepsilon_R = 6\%$, $\sigma_R = 4.5$ MPa), the dislocation density is still high ($\simeq 10^{10}$ cm^{-2}). The mean size of the rod-shaped precipitates retains the same order of magnitude as above (100 nm × 1000 nm) and the rounded small precipitates are not visible (Fig. 11a, b). The precipitation fine structure has disappeared and has changed into a coarser precipitation.

These observations on strained samples point to two main results about precipitation structure.

(i) The rod-shaped precipitate density is higher in the composite than in the reinforced material. Their size is similar in both matrix and composite. Small rounded precipitates are present in the matrix but are not visible in the composite.

(ii) The nucleation of the precipitates during the high-temperature tensile deformation tests seems to be favoured by the fibre reinforcement.

Comparing T6 and strained samples, it is concluded that the precipitation structure is much coarser after a high-temperature tensile test (compare Figs 7 and 8, and 9–11). We think that this result originates from the combined action of strain and temperature. In another way, the importance of a thermal treatment is emphasized: it is shown that it has a basic influence on the precipitation structure and, consequently, on the mechanical behaviour of the material.

4. Conclusions

The rod-shaped precipitates observed in the studied material have a hexagonal structure with parameters $a = 0.42 \pm 0.01$ nm and $c = 0.68 \pm 0.015$ nm which does not correspond to the values usually reported for Mg_2Si. Moreover, their chemical composition (atomic ratio Mg/Si $\simeq 1$) is not consistent with Mg_2Si stoichiometry.

Microhardness measurements and TEM observations agree with the conclusion that the hardening kinetics is enhanced by the presence of fibre reinforcement of the matrix alloy during a T6 treatment. We explain this feature by differences in thermal expansion coefficients of the matrix and fibres which induces plastic deformation during temperature variations. A higher dislocation density in the reinforced material supplies preferential precipitation sites and plastic deformation enhances diffusion.

When a high-temperature deformation test is added to thermal treatment, coarsening of the precipitation is still more evident.

References

1. B. COUTAND, F. GIROT, Y. LEPETITCORPS and J. M.

QUENISSET, in "Proceedings ECCM 4", Bordeaux, March 1989, edited by A. R. Bunsell *et al.*, (1989) pp. 16–17.
2. C. BRICHET, Thèse Ingenieur-Docteur, Université de Paris-Sud (1971).
3. M. H. JACOBS, *Phil. Mag.* **26** (1972) 1.
4. S. D. DUMOLT, D. E. LAUGHLIN and J. C. WILLIAMS, *Scripta Metall.* **18** (1984) 1347.
5. F. GIROT, J. M. QUENISSET, R. NASLAIN, B. COUTAND and T. MACKÉ, in "Proceedings of ICCM VI-ECCM2", July 1987, London, edited by F. L. Matten (1987) pp. 330–39.
6. T. CHRISTMAN and S. SURESH, *Acta Metall.* **36** (1988) 1691.

Received 12 February
and accepted 20 June 1991